Accepted Manuscript

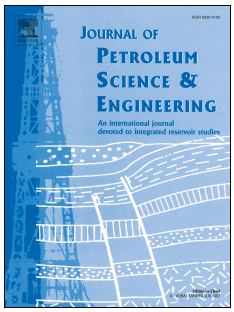

The effect of pore structure on non-Darcy flow in porous media using the lattice Boltzmann method

Zhilin Cheng, Zhengfu Ning, Qing Wang, Yan Zeng, Rongrong Qi, Liang Huang, Wentong Zhang

PII: S0920-4105(18)30821-0

DOI: 10.1016/j.petrol.2018.09.066

Reference: PETROL 5329

To appear in: *Journal of Petroleum Science and Engineering*

Received Date: 11 July 2018

Revised Date: 22 August 2018

Accepted Date: 21 September 2018

Please cite this article as: Cheng, Z., Ning, Z., Wang, Q., Zeng, Y., Qi, R., Huang, L., Zhang, W., The effect of pore structure on non-Darcy flow in porous media using the lattice Boltzmann method, *Journal of Petroleum Science and Engineering* (2018), doi: https://doi.org/10.1016/j.petrol.2018.09.066.

The effect of pore structure on non-Darcy flow in porous media using the lattice Boltzmann method

Zhilin Cheng [a,b,*], Zhengfu Ning [a,b*],Qing Wang [a,b], Yan Zeng [c], Rongrong Qi [a,b], Liang Huang [a,b], Wentong Zhang [a,b]

a State Key Laboratory of Petroleum Resources and Engineering, China University of Petroleum-Beijing, Beijing 102249, China

b School of Petroleum Engineering, China University of Petroleum-Beijing, Beijing 102249, China

c Institute of Mechanics, Chinese Academy of Sciences, Beijing 100190, China

Abstract

Non-Darcy flows associated with high Reynolds numbers often occur in the near-wellbore regions of gas reservoirs or hydraulic fractures and thus should not be ignored. However, investigating non-Darcy flow in these porous rocks through laboratory experiments is always expensive and time-consuming. As such, this article sought an alternative method, and a lattice Boltzmann study of non-Darcy flow in various porous models was performed. The applicability of two non-Darcy correlations in porous media and the effect of pore structure on non-Darcy flow were examined. In addition, the reasons for the deviation from the linear Darcy flow and different flow patterns related to inertial effects of the fluid were also studied. The results showed that the characterization of non-Darcy flow in porous media with the cubic law can only be valid in a narrow range of Reynolds number beyond the Darcy regime, outside of which the strong inertia-dominated flow yields to the quadratic correction. On the whole, representing the non-Darcy flows using the quadratic correction is acceptable, especially for porous media with a higher complexity. The features of non-Darcy flow greatly depend on the pore structure of a porous medium, and more heterogeneous pore models always have a faster cessation for Darcy flow and a higher β factor. Furthermore, for simple porous media a small amount of parameters may be adequate for the prediction of the β factor; while the correlations involving more parameters would

be needed to determine the β factor for more intricate porous models, although such correlations may not be widely used in various industries. Besides, the non-Darcy flow that occurs in porous media is collectively controlled by different mechanisms. At elevated velocities, the inertial core effect in a large channel will lead the flow to be more homogeneous and less tortuous, while in porous models with complicated pore space, the steady eddy and reversal flow resulting from drag force will make the flow paths more tortuous. As such, it is the hope of this study to provide some new insights into the non-Darcy flow in porous media.

Keywords: Porous media; Pore structure; Darcy flow; Non-Darcy flow; Lattice Boltzmann method

1. Introduction

As the most important discipline in the description of fluid transport in porous media, Darcy's law has been widely adopted in petroleum industries. Darcy flow is also known as the creeping flow, an event which takes place in porous materials at a very low Reynolds number (Re <<1). For the increase in flow rates, such as the fluid flow in the near-wellbore regions of high-capacity gas and condense reservoirs (Thauvin and Mohanty, 1998) or in proppant-filled hydraulic fractures, Darcy's law no longer holds due to the effect of fluid inertia (Andrade Jr et al., 1999), here the fluid governing equation can be corrected with a quadratic or cubic term, and the commonly used correlation is the quadratic correlation (Forchgeimer equation) (Forchheimer, 1901):

$$-\nabla p = \frac{\mu}{K_f} U + \beta \rho U^2 \tag{1}$$

Where ∇p is the pressure gradient in the specific direction, Pa/m; μ is the dynamic viscosity of the fluid, Pa·s; ρ is the density of the fluid, kg/m^3. In addition, U is the mean velocity through the porous medium, m/s. K_f is the Forchheimer permeability which is very close but not equal to Darcy permeability (Balhoff and Wheeler, 2009; Muljadi et al., 2016; Newman and Yin, 2013), mD; β is termed as the inertial coefficient or beta factor, m^{-1}. Note that both the Darcy flow and non-Darcy flow belong to stationary flows; as Reynolds number increase further, the flow will enter the unsteady

turbulent regime, which is out of scope of this article. Also, turbulent flow rarely occurs in subsurface problems (Balhoff and Wheeler, 2009).

Investigating the inertial non-Darcy flow through porous media is essential for gas reservoirs modeling and the productivity evaluations of fractured gas wells (Friedel and Voigt, 2006; Miskimins et al., 2005; Ramirez et al., 2007). Generally, the β factor and the onset of non-Darcy can be measured through careful multi-rate pressure tests performed on relatively large rock samples (Chukwudozie and Tyagi, 2013; Macini et al., 2011), Zeng and Grigg (Zeng and Grigg, 2006) recommended a revised Forchheimer number to identify the beginning of the non-Darcy flow, and discussed the applicability of that through conducting gas flow experiments on several consolidated rocks. Macini et al. (Macini et al., 2011) reported a series of experiments performed on natural and artificial unconsolidated porous media, showing the significant impact of pore structure (grain size distribution and porosity) on fluid flow through porous media. But it is evident that the experimental methods are always rather time-consuming and expensive. It is thus of great interest to numerically explore the non-Darcy flow in porous models at pore scale through solving the discretized Navier-Stokes (NS) equation. Indeed, the macroscopic flow properties can be obtained by averaging the entire simulation domain. Previous studies (Fourar et al., 2004; Hill et al., 2001; Koch and Ladd, 1997; Narváez et al., 2013; Yazdchi and Luding, 2012; Yazdchi et al., 2010) have examined non-Darcy flows in simplified porous geometries, which are often constituted by rectangles, circles, cylinders, eclipses or spheres. Furthermore, conceptual pore network modeling was also used for the investigation of non-Darcy flow. For instance, Wang et al. (Wang et al., 1999) proposed a tensorial Forchheimer equation that was verified by a novel pore network simulation. Then, they evaluated the contribution of non-Darcy components with three anisotropic models. Considering that the pore structure of these kind of models are quite different from that of natural rock materials, recently investigators have studied the fluid flow within pore spaces in either stochastically reconstructed samples or computed tomography (CT) samples that have been directly obtained. Chukwudoize and co-workers (Chukwudozie and Tyagi, 2013; Chukwudozie et al., 2012) used the lattice Boltzmann method (LBM), combined with the non-Darcy flow theory, to estimate the permeability, tortuosity, and the β factor of a

periodic body centered by cubic arrays of smooth and rough sphere packs, along with 3D CT images of realistic porous rocks. By comparing these computed properties to experimental data, they found a good agreement. Furthermore, they also briefly demonstrated the effects of roughness on inertial flow in porous media. In addition, a recently direct pore-scale study done by Muljadi et al. (Muljadi et al., 2016) emphasized the effects of structural heterogeneity on the onset of non-Darcy flows and β factor with three kinds of porous media. Newman and Yin (Newman and Yin, 2013) adopted the LBM for performing a detailed study of non-Darcy flows in synthetic 2D media, with a porosity range of 8-35 %, and they demonstrated that the contrast between pore and throat size prompted the transition to inertial flows. Through performing a number of LB flow simulations in various porous media, Arabjamaloei and Ruth (Arabjamaloei and Ruth, 2017) showed that the apparent permeability reduction was due to inertial effects and they also provided a new empirical correlation to predict the scaled permeability change of a porous medium. Nissan and Berkowitz (Nissan and Berkowitz, 2018) employed an FEM for the simulation depicting fluid flow through 2D pore-scale matrices with various pore structures to investigate the inertial effect on flow and transport, and they found that the inertial flow behavior was controlled by the medium structure and more heterogeneous models would magnify the inertial effect.

Thus far, extensive research has revealed that macroscopic flow behaviors are associated with the pore structure. However, a quantitative study to shed light on the effects of several microstructural parameters on macroscopic permeability and β factor is still lacking. Moreover, although media with simple geometries may bear little resemblance to natural porous materials, it is amendable, and such models can be used to implement sensitivity analysis for structure complexity due to the well-adjustability of its structural parameters (Yazdchi and Luding, 2012; Yazdchi et al., 2011; Yazdchi et al., 2012). The results of this can then also be favorable to the development of the empirical equation to predict the transport properties of fluid. On the other hand, similar to apparent permeability, the tortuosity of a porous medium is also varied with entering the non-Darcy flow regime, which can be responsible for the variation in the flow patterns of fluids in pore space. However, its actual dependence on complex geometries and topologies is not well understood. For instance, in the study of Muljadi et al. (Muljadi et al., 2016), a typically inertial structure, steady eddies

was not formed within the beadpack and Benthimer sandstone, but occurred in Estaillades carbonate. A similar phenomenon was also found in Ref (Andrade Jr et al., 1999). Furthermore, the change of tortuosity can reflect the variety of flow paths in porous media. However, most of the works reported an increase of tortuosity at elevated flow rates. To our knowledge, only Yazdchi and Luding (Yazdchi and Luding, 2012) presented an opposite trend for the variation of tortuosity, but they did not elaborate on that further. As such, the nature of the varying tortuosity remains unclear. Collectively, these studies clearly outline a critical role for the effects of pore structure on the characteristics of non-Darcy flows. However, a systematic understanding of how structural properties influence the non-Darcy flow in diverse porous media, including both simple geometry models and complicated porous media, is still needed.

The objectives of this research were thus to explore the non-Darcy flows in porous media with various pore complexities through the use of LBM. By conducting the flow simulations, the applicability of the Forchheimer equation was confirmed, and the effects of some relevant structural parameters on the onset of non-Darcy and β factor was quantitatively examined. Additionally, the mechanisms of varied tortuosity in non-Darcy flow were also clarified. The remaining part of the present study will proceed as follow: The lattice Boltzmann model was briefly introduced in Section 2. Along with this, Section 2 will also show the algorithm used for generating different porous media and the more detailed non-Darcy flow theory were presented. In Section 3, the β factor and the onset of non-Darcy flow were calculated, and the influence of the pore structure's effect, the change of tortuosity, and associated flow patterns were discussed in detail. Finally, some conclusions are drawn in Section 4.

2. Theory and numerical methods

2.1 Lattice Boltzmann method

The original Boltzmann equation cannot be directly solved due to its high-order nonlinear nature. Rather, a commonly used method is the use of an approximate model for the Boltzmann equation, namely the BGK approximation (Bhatnagar et al., 1954), which is also known as the single relaxation time (SRT) model. An alternative solution is the

multiple relaxation time (MRT) method, which incorporates multiple collision operators to increase the stability and accuracy of the simulation. Although compared with the SRT model, the MRT method shows a 30% increase in computational time (Newman and Yin, 2013), it has been widely used to study single phase flow and multiphase flow in porous materials due to its high accuracy and the well-adjustability of the relaxation time (Chen et al., 2014; Zhao et al., 2017; Zhao et al., 2018a; Zhao et al., 2018b; Zhao et al., 2018c). In this study, the MRT-LBM was employed to simulate the Darcy flow and inertial flow in porous media. The standard LB equation with the MRT collision operators is expressed as

$$\mathbf{f}(\mathbf{x}+c\mathbf{e}\Delta t, t+\Delta t)=\mathbf{f}(\mathbf{x},t)-(\mathbf{M}^{-1}\mathbf{S}\mathbf{M})(\mathbf{f}(\mathbf{x},t)-\mathbf{f}^{eq}(\mathbf{x},t)) \tag{2}$$

Where $\mathbf{f}(\mathbf{x},t)$ is the fluid density distribution function at lattice site **x** and time *t*; c is the lattice speed which equals $\Delta x/\Delta t$ with Δt being the lattice time step, as both of them are generally set as a unity. For the D2Q9 model, the lattice discrete velocities **e** of a given point was given by (Qian et al., 1992)

$$\mathbf{e}=\begin{pmatrix} 0 & 1 & 0 & -1 & 0 & 1 & -1 & -1 & 1 \\ 0 & 0 & 1 & 0 & -1 & 1 & 1 & -1 & -1 \end{pmatrix} \tag{3}$$

The equilibrium distribution function $f_i^{eq}(\mathbf{x},\mathrm{t})$ is written as (Qian et al., 1992)

$$f_i^{eq}=\rho\omega_i\left[1+\frac{3}{c^2}(\mathbf{e}_i\cdot\mathbf{u})+\frac{9}{2c^4}(\mathbf{e}_i\cdot\mathbf{u})^2-\frac{3}{2c^2}\mathbf{u}^2\right] \tag{4}$$

In the above equation, ω_i is the weight factor associated with different lattice velocities and can be given by $\omega_0=4/9$, $\omega_{1\text{-}4}=4/9$ and $\omega_{5\text{-}8}=1/36$. In addition, the fluid velocity and density are calculated through the Equation (4). It is to be noted that, in this work, the Mach number (the ratio of fluid velocity to the sound speed) was kept below 0.1 to minimize the compressibility effect of flow (Feng et al., 2007; Newman and Yin, 2013).

$$\rho=\sum_i f_i \tag{5a}$$

$$\rho\mathbf{u}=\sum_i \mathbf{e}_i f_i \tag{5b}$$

In addition, **M** is the velocity vector transformation matrix to momentum constructed by (Guo et al., 2002b; Yu and Fan, 2010)

$$\mathbf{M} = \begin{pmatrix} 1 & 1 & 1 & 1 & 1 & 1 & 1 & 1 & 1 \\ -4 & -1 & -1 & -1 & -1 & 2 & 2 & 2 & 2 \\ 4 & -2 & -2 & -2 & -2 & 1 & 1 & 1 & 1 \\ 0 & 1 & 0 & -1 & 0 & 1 & -1 & -1 & 1 \\ 0 & -2 & 0 & 2 & 0 & 1 & -1 & -1 & 1 \\ 0 & 0 & 1 & 0 & -1 & 1 & 1 & -1 & -1 \\ 0 & 0 & -2 & 0 & 2 & 1 & 1 & -1 & -1 \\ 0 & 1 & -1 & 1 & -1 & 0 & 0 & 0 & 0 \\ 0 & 0 & 0 & 0 & 0 & 1 & -1 & 1 & -1 \end{pmatrix} \tag{6}$$

S is a diagonal relaxation matrix in moment space **M**:

$$\mathbf{S} = \mathrm{diag}[s_1,\ s_2,\ s_3,\ s_4,\ s_5,\ s_6,\ s_7,\ s_8,\ s_9] \tag{7}$$

The selection of the parameters in Equation (7) follows the Ref (Huang et al., 2014), i.e., $s_1 = s_4 = s_6 = 1.0$, $s_2 = 1.64$, $s_3 = 1.54$, $s_5 = s_7 = 1.2$ and $s_8 = s_9 = 1/\tau$; in which, the relaxation time τ is, safely set as unity. The kinetic viscosity is also related to the relaxation time, and the sound speed c_s ($= c/\sqrt{3}$), defined by:

$$\nu = c_s^2(\tau - \frac{1}{2})\Delta t \tag{8}$$

Furthermore, boundary conditions in this paper contain the standard bounce-back scheme and non-equilibrium extrapolation boundary condition (Guo et al., 2002a); herein, the former was used to treat the fluid-solid boundary, while the latter was applied in the inlet and outlet boundaries of the model to assign the specified pressure difference.

Finally, the conversion of the LBM dimensions to physical units can be simply determined by three characteristic factors, i.e., length (L_0), time (T_0) and mass (M_0). Since the values of the domain size, fluid density, and kinetic viscosity for both the LBM and physical systems are known, these characteristic factors can be calculated using the following relationships,

$$L_0 = \Delta x_p / \Delta x \tag{9a}$$

$$T_0 = \nu L_0^2 / \nu_p \tag{9b}$$

$$M_0 = L_0^3\, \rho_p / \rho \tag{9c}$$

Note that the subscript "*p*" represents the physical dimension, while the variable without a subscript would mean the lattice space, unless otherwise stated. Once L_0, T_0 and M_0 are determined, other physical parameters can be easily obtained, e.g. pressure, velocity, permeability, etc.

2.2 2D porous media generation

The characterization of fluid flow in porous media is challenging. Aside from the fact that it commonly involves multiple mechanisms, an important factor is that its flow or transport properties are usually dependent on the pore structure of the porous medium. In this study, two groups of geometry models were adopted for the simulation of the fluid flow.

One is the porous models constituted by a certain amount of round particles with an equal diameter. This kind of geometry models is normally regarded as the benchmark for the non-Darcy flow in porous media because of its simplicity (Hill et al., 2001; Koch and Ladd, 1997; Yazdchi and Luding, 2012). Eight geometry models were created by randomly placing particles into the computational domain that was 500×300 lattices in size, until the expected porosity was achieved. Additionally, the minimum distance of any two particles is set as 2.2R to inhibit the overlap of grains, in which R is the particle radius. The detailed geometry parameters used in this paper are listed in Table 1. It is worth noting that the size of the grain model differs from the system size in Table 1, and the main reason for this will be discussed later in section 3.1.

Table 1

Properties of the generated porous media: structural information, porosity, specific surface area.

Geometry model	No.	R (μm)	System size	Poro	SSA (um^{-1})
C1	144	12	1000×600	0.577	0.107
C2	89	15	1000×600	0.579	0.086
C3	63	18	1000×600	0.576	0.073
C4	51	20	1000×600	0.573	0.067
C5	383	6	1000×600	0.712	0.115
C6	259	8	1000×600	0.66	0.115
C7	187	10	1000×600	0.605	0.115

C8	150	12	1000×600	0.559	0.115
R1	-	-	1500×900	0.393	0.088
R2	-	-	1500×900	0.736	0.059
R3	-	-	1500×900	0.577	0.079
R4	-	-	1500×900	0.799	0.075

No. : the number of particles; R: radius of the particle; Poro: porosity of the geometry; SSA: specific surface area.

The examples of the geometry models, C4 and C8, are displayed in Figure 1a and 1b, where no overlap grains exist and the white zone represents the pore phase, whereas black represents the solid obstacle.

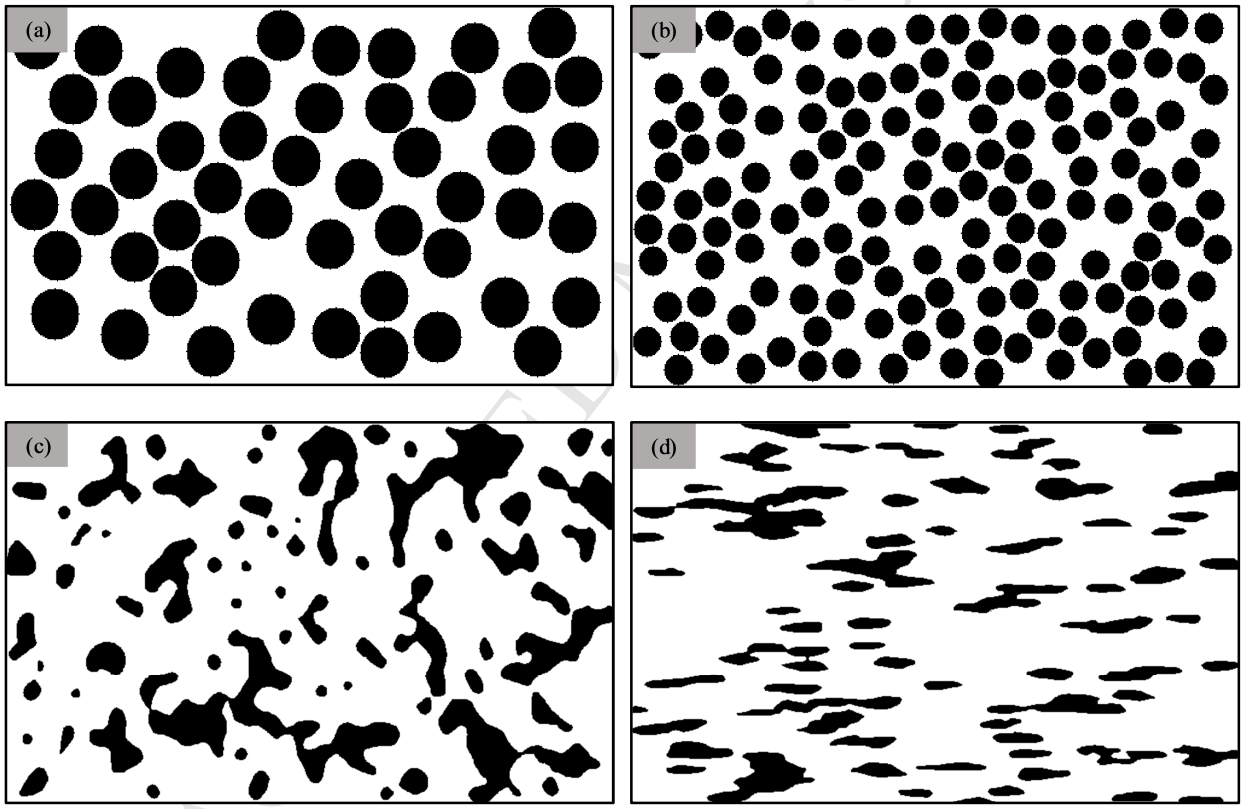

Fig.1. Examples of pore media studied in this paper. (a), (b), (c) and (d) represent the configuration of C4, C8, R2 and R4 respectively. The remaining models are presented in our supplementary materials Figure S1.

The generation of the other four geometries were accomplished using the Quartet Structure Generation Set (QSGS) algorithm developed by Wang et al. (Wang et al., 2007). The QSGS is a stochastic method which mainly incorporates four parameters: core distribution probability, directional growth probability, phase interaction growth probability and

volume fraction of each phase. For more details about this algorithm, one may refer to Ref (Wang et al., 2007). Through the adjustment of these variables, different types of porous media can be obtained. Furthermore, for the system with only one growth and one non-growth phase, the phase interaction growth probability can be neglected.

Here, based on a blank domain with the size of 500×300 lattice nodes, we set different directional growth probabilities and fractions of growth phase for each model to generate four distinctive geometries, with the graphs of model R2 and R4 as examples, which are also plotted in Figure 1. It is observed that for R2, the solid phase favored growing in a longitudinal direction while the solid in R4 was prone to development in horizontal direction. Note that after these porous media were reconstructed, the median filter and the connected phase labeling algorithm (Chen et al., 2015) were applied to identify the effective flow paths, as the isolated pores have little contribution to fluid flow in pore space. It is also to be noted that both the grain structure models and the reconstructed porous media have an identical physical size of 500×300 μm^2.

2.3 Non-Darcy flow theory

Based on the simulation results from LBM, the primary characteristics of the non-Darcy flow can be readily determined. Darcy law is used to acquire the intrinsic permeability of a porous medium. At elevated velocities, the flow in porous media is dominated by the fluid inertia, and as such, the linear relationship between the pressure gradient and the superficial velocity is broken down. Several attempts have been made to quantify the additional pressure drop caused by the inertial resistance. Besides the popular correlation (Forchheimer equation), another alternative is the cubic law (Firdaouss et al., 1997; Marusic-Paloka and Mikelic, 2000; Mei and Auriault, 1991), which is defined as

$$-\nabla p = \frac{\mu}{K_d} U + aU^3 \tag{10}$$

Where a is a constant; and K_d is the Darcy permeability, mD. Certain scholars (Newman and Yin, 2013) have demonstrated that Equation (10) is only valid in a weak inertial flow with a narrow range of velocities. Beyond this regime, the fluid flow yields the Equation (1).

In addition, the Re is typically used to characterize the transition from Darcy flow to non-Darcy flow, which reflects the

ratio of inertial force and viscous effects, and a common definition is

$$\mathrm{Re} = \frac{\rho U d}{\mu} \tag{11}$$

In this definition, d is the average diameter of the grains, m; but for a highly disordered medium, d is difficult to determine and is inadequate for the representation of the pore structure characteristic. Hence, another formulation (Muljadi et al., 2016; Newman and Yin, 2013) was adopted in this study, as described by Equation (12)

$$\mathrm{Re} = \frac{\rho U \sqrt{K_d}}{\mu} \tag{12}$$

Through combining Equation (1), (10) and (12), a generalized non-dimensional form of non-Darcy flow equation can be derived, which is similar to the formulation introduced by Yazdchi and Luding (Yazdchi and Luding, 2012) (see Equation (13))

$$f^{'} = 1 + \gamma \mathrm{Re}^{\lambda} \tag{13}$$

Where the friction factor is $f^{'} = K_d/K_{app}$, and the apparent permeability is $K_{app} = -\nabla p/(\mu U)$, mD. For quadratic term equation, $\gamma = \beta\sqrt{K_d}$ and λ=1. Likewise, λ equals two for the cubic correction.

Furthermore, β is often calculated by setting a cut-off in the plot and fitting the inertia-dominated flow to obtain the slope (Chukwudozie and Tyagi, 2013; Chukwudozie et al., 2012; Muljadi et al., 2016; Newman and Yin, 2013). We suggest this method could lead to some errors, especially when there is less simulation data. Here, β is directly determined by fitting all data with Equation (13).

The effect of tortuosity (namely τ) on β factor has been highlighted by some researchers (Chukwudozie et al., 2012; Cooper et al., 1999; Kakouei et al., 2017), and is defined by (Duda et al., 2011; Koponen et al., 1996)

$$\tau = \frac{\langle U \rangle}{\langle U_x \rangle} \tag{14}$$

Where $\langle U_x \rangle$ is the spatial average of the fluid velocity along the macroscopic flow direction, whereas $\langle U \rangle$ is termed as well as the previous definition.

3. Results and discussion

In this section, a series of LBM simulations was performed in order to investigate fluid flow in grain structures and stochastically generated porous media. In the following simulations, the bounce-back (no-slip) boundary condition is applied both at the top and bottom of the system, as well as the surface of the obstacles, and the pressure is set on the left and right. The features of Darcy and non-Darcy flow in pore space were captured by gradually varying the pressure difference between the inlet and the outlet. Note that our numerical models have been validated in our supplementary materials, which include Darcy flow and non-Darcy flow simulations.

3.1 Grid refinement analysis

A sufficiently fine grid is exceptionally crucial for mimicking fluid flow within samples with complex pore space or relatively high Reynolds number. More pore space would be likely to be created for fluid flow with the grid domain being refined (Chukwudozie et al., 2012; Muljadi et al., 2016). Therefore, in order to acquire a credible understanding of non-Darcy flows in porous media, one must make sure that the grid resolution is adequate.

Given that two sets of samples with diverse pore structures were used, we selected C8 and R1 to check the grid coverage in the LBM simulations, owing to their low permeabilities and high SSA. Through subdividing a pixel into four and nine smaller pixels, the original model can be enlarged to a finer geometry with either 1000×600 or 1500×900 elements. Several simulations were re-run at different grid resolutions, and the results are shown in Figure 2. One can see that the mesh resolution has a significant effect on the fluid flow in porous media; the original grid density is insufficient for revealing the feature of the non-Darcy flow, or even the Darcy flow, because the effective flow channels cannot be resolved. This includes, for instance, at lower Reynolds number, where the Darcy permeability is evidently lower than that at higher mesh resolutions. The trends of the apparent permeability varying with an increase in the Reynolds number under two refined grids are perfectly matched for C8, indicating that a grid resolution of 1000×600 pixels is sufficient for the description of non-Darcy flow in porous media. Although there is a difference in simulation results under the two refined ones for R1, the minor deviation is acceptable. The mesh density of 1500×900 pixels was

used safely in conducting the following simulations, with respect to the second group of porous models, as can be seen in Table 1.

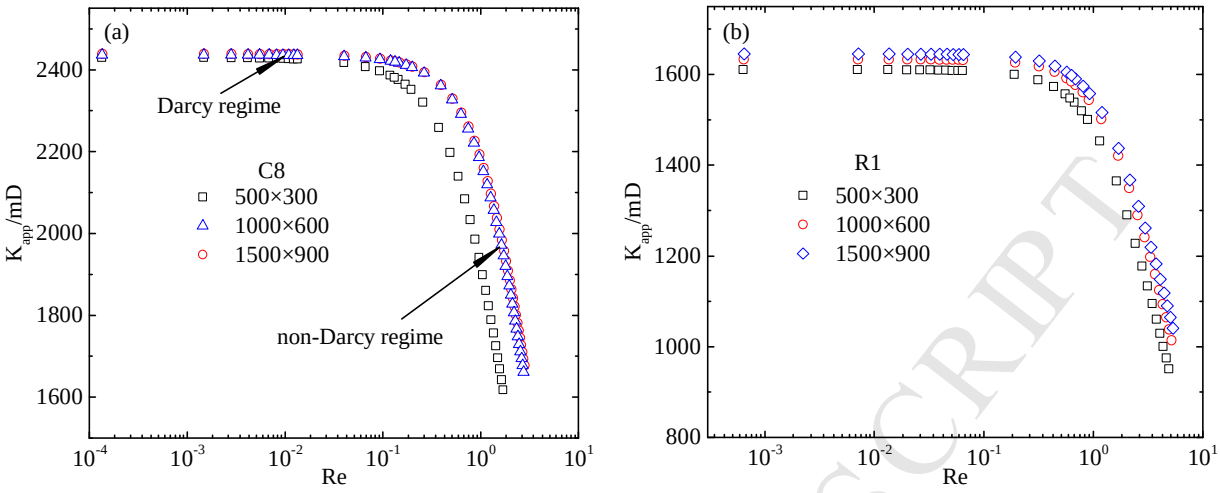

Fig.2. The variation of apparent permeability as a function of Reynolds number for (a) C8 and (b) R1 at different grid resolution.

3.2 Characterization of non-Darcy flow in porous media

On the basis of the theory given in section 2.3, some relevant parameters can be determined for the identification of non-Darcy flows. For very low velocities, i.e., the creeping flows, the Darcy permeabilities of all the models have been summarized in Table 2. The permeabilities for C1~C8 has a narrow range from 2436 to 8893 mD, while only four permeabilities for R1~R4 exhibit a large fluctuation between 1645 to 40137 mD, which could be due to the substantial variation in pore structures. Plus, the tortuosities of various geometries can be calculated from the entire velocity filed distribution, which is also seen in Table 2. The tortuosity is able to reflect the heterogeneity of a porous medium to some degree; the values of most of these models are approximately 1.2. It is also found that R1 has the lowest permeability but has the highest value of tortuosity. In contrast, R4 has the highest permeability but minimal tortuosity. However, it would seem that there is no monotonous connection that exists between the permeability and the tortuosity. In addition, it should be noted that the permeability and tortuosity would change as the Re increases up to an inertial flow; as such, their listed values would correspond to the Darcy regime.

Table 2

The acquired results fitted by quadratic and cubic non-Darcy correlations. Note that the equations shown in Table 2 correspond to the quadratic fitting because of the higher *R* Square.

Geometry model	R^2		Fitting equations	β ($\times 10^3$ m^{-1})	τ	Perm (md)
	λ=1	λ=2				
C1	0.990	0.949	y=1+0.3045x	166.88	1.236	3329.4
C2	0.991	0.947	y=1+0.2622x	116.63	1.203	5053.3
C3	0.990	0.959	y=1+0.2855x	112.35	1.201	6459
C4	0.992	0.931	y=1+0.2402x	80.39	1.176	8893.3
C5	0.983	0.962	y=1+0.1202x	56.90	1.147	4464.6
C6	0.988	0.953	y=1+0.1652x	78.49	1.213	4427.4
C7	0.991	0.944	y=1+0.1889x	101.11	1.244	3491.6
C8	0.984	0.962	y=1+0.2798x	179.25	1.231	2436.3
R1	0.997	0.917	y=1+1.7193x	1340.54	1.545	1645
R2	0.997	0.907	y=1+0.6234x	205.30	1.227	9219.9
R3	0.992	0.945	y=1+0.4350x	128.25	1.216	11505
R4	0.995	0.903	y=1+0.0757x	11.95	1.072	40137

R^2: the coefficient of determination; Perm: permeability of the porous medium.

With the increase of velocity in pore space, the flow regime progressively transforms from a Darcy flow to non-Darcy flow, and the flow equation can be modified through a quadratic correlation. However, to further investigate the application of Equation (1) and (10) in characterizing the non-Darcy flow, the graph of the friction factor versus Reynolds number of each model were all fitted by those two relations. As can be seen from Table 2, in terms of all the models, the quadratic term (λ=1) has a better accuracy than the cubic one (λ=2) due to the higher R^2. Furthermore, it appears that the Forchheimer equation might have a better applicability in the constructed models with the QSGS

method, where all the R^2 values are >0.99.

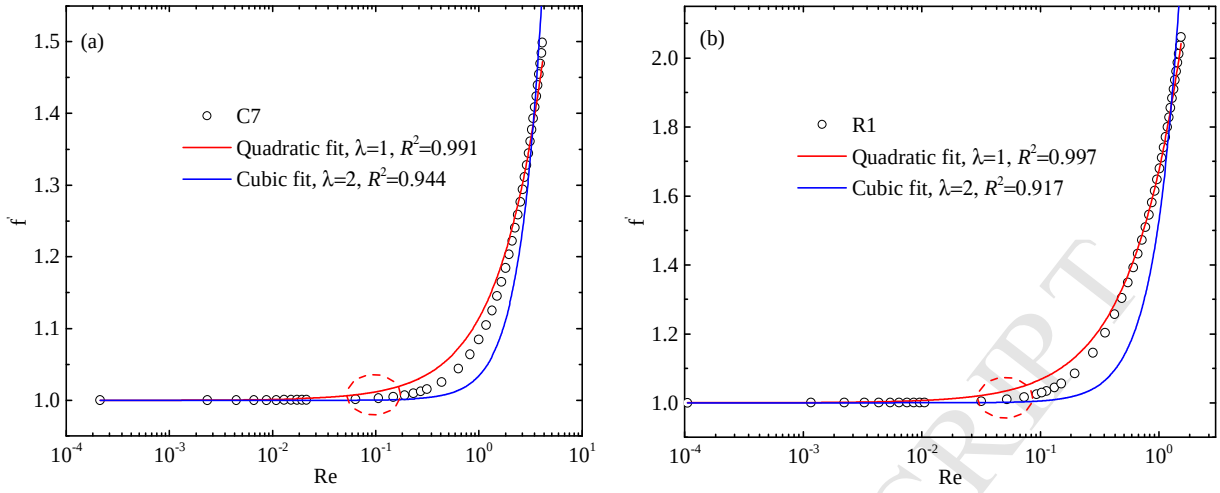

Fig.3. The plots of the friction factor versus Re and fitted lines for (a) C7 and (b) R1, using quadratic and cubic correlations.

Taking the cases of C7 and R1 as an example, the simulation results and the fitting lines are shown in Figure 3. It is revealed that the cubic law can indeed be used to represent the weak inertial flow, i.e., the early stage of non-Darcy flows, whereas the quadratic correction is more appropriate for the strong inertial regime. This finding is in accordance with the conclusions of previous authors (Fourar et al., 2004; Koch and Ladd, 1997; Newman and Yin, 2013). Nevertheless, the cubic law only applies to a narrow range of Reynolds number (see the inserted circular in Figure 3). In its entirely, the whole flow regime, as represented by the Forchheimer equation, is acceptable. On the other hand, when the fitting equations are known, the β factor can be easily derived (see Table 2). It would appear that no obvious regularity was able to be observed between the β factor and other parameters due to the scattered nature, implying that the β factor is controlled by multiple factors that will be discussed in what follows.

3.3 The impacts of pore structure on non-Darcy flow

The pore structure of a porous medium greatly affects the flow in pore space and results in a challenge for the determination of the primary properties of non-Darcy flows, both macroscopically and microscopically. An advantage of generating grain models is that we can shift one specific geometrical parameter, while simultaneously, being able to fix the other relevant ones freely. For simplicity, this section illustrates the effects of specific surface area and porosity

(structural parameters can be seen in Table 1) on non-Darcy flow.

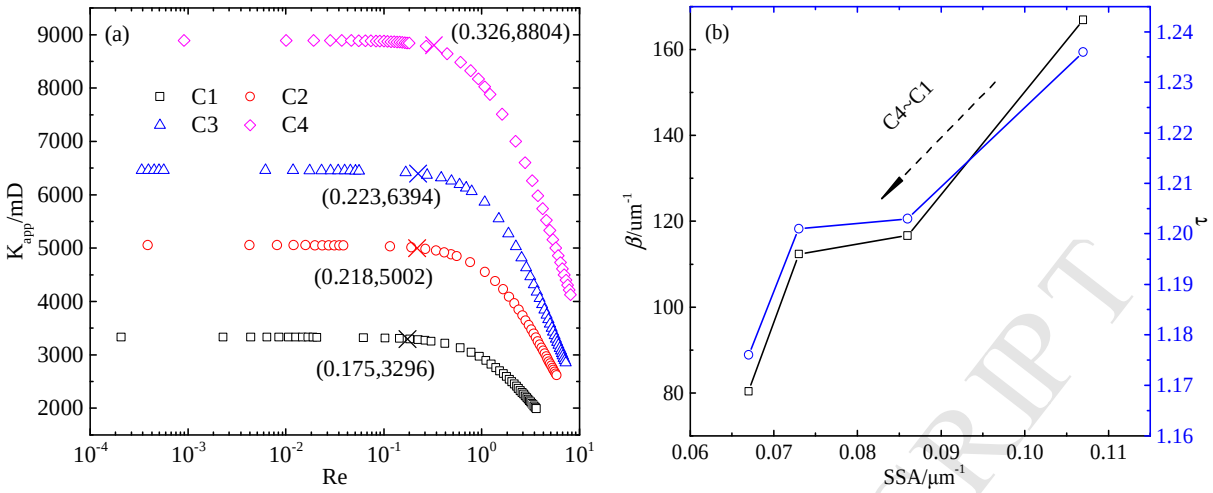

Fig.4. The effect of specific surface area on non-Darcy flow. (a) The plot of apparent permeability versus Reynolds number at various SSA; (b) Variation of the β factor and tortuosity as a function of SSA.

As shown in Figure 4, the variation tendency of apparent permeabilities for these models experiences a smooth phase, i.e. the Darcy regime, until the point of deviation, which is called the onset of the non-Darcy flow. Then, at elevated velocity circumstances, the fluid flow is dominated by the inertial effect, which results in a decline in the apparent permeability. Different criteria have been proposed by several authors (Comiti, 2000; Ma and Ruth, 1993; Zeng and Grigg, 2006) in identifying the cession of the Darcy flow, and a commonly used limit is the definition suggested by Comiti (Comiti, 2000), who identified this cessation at the point when the pressure drop due to the linear term becomes less than 99% of the total. In other words, once the friction factor $f^{'}$ is more than 1.01, the Forchheimer regime is assumed. The onset of the non-Darcy flow is marked by a cross symbol, as depicted in Figure 4a, and indicates that a decreasing trend in the porous medium with a low permeability is more rapid compared to one with a higher permeability, a statement that is in a good agreement with the previous numerical results (Chukwudozie and Tyagi, 2013; Kakouei et al., 2017; Muljadi et al., 2016). Furthermore, it can be found from Figure 4b that for the same porosity, a porous medium with a larger SSA leads to a lower permeability and larger β factor and tortuosity. This is as for the porous media with similar structural characteristics; a larger SSA generally leads to a more complex and tortuous pore structure.

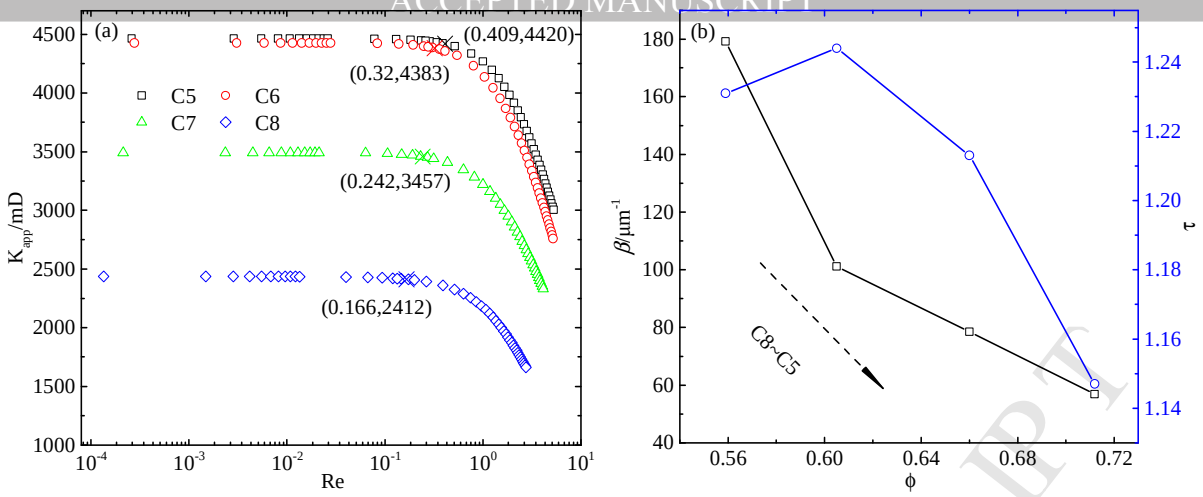

Fig.5. The effect of porosity on non-Darcy flow. (a) The plot of apparent permeability versus Reynolds number at different porosities; (b) Variation of the β factor and tortuosity as a function of porosity.

Similarly, as expected, in the same SSA, the porous model with a low permeability would mean the a less effective pore space available for fluid flow. Thus, a smaller value of the onset of non-Darcy flow is observed for such a model, as shown in Figure 5a. We also notice that if based on the observation of the cases C7 and C8, a large contrast in the permeability for them results in the significant differences in their β factor and onset value of inertial flow. However, while models C5 and C6 have rather similar permeability, the differences in the β factor and the onset value for inertial flow of both are relatively large, revealing that permeability are not purely controlled by the effective porosity. Additionally, there is a clear trend of a decrease in the β factor with increasing the porosity of the geometry, while no obvious correlation was found between the tortuosity and porosity (see Figure 5b).

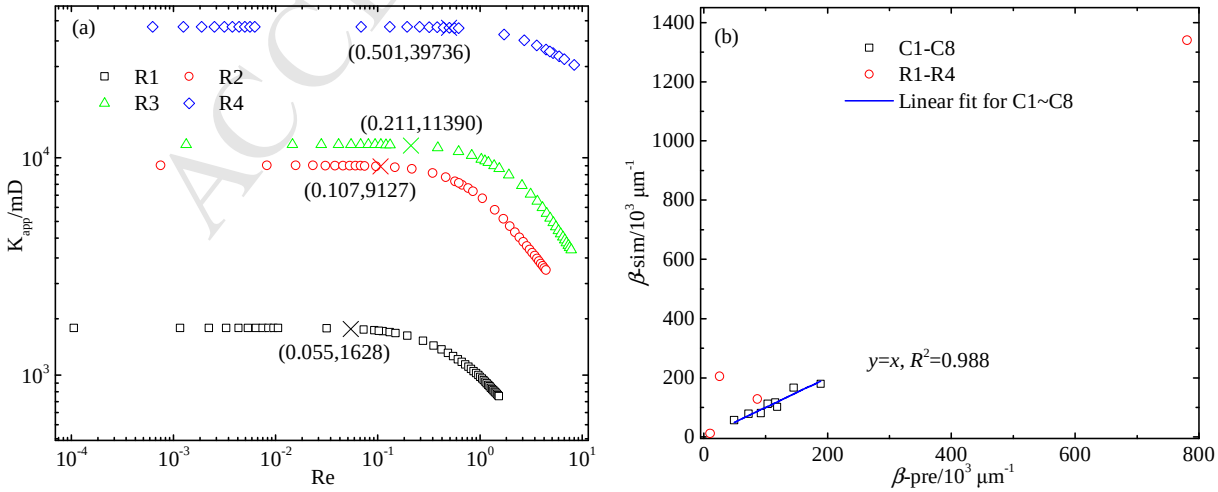

Fig.6. Non-Darcy flow in stochastically constructed porous media. (a) The plot of apparent permeability versus

Reynolds number; (b) The relationship between the β factor and the defined non-Darcy factor Nf for various models.

As for the naturally porous media, including the stochastically generated models, it would be impossible to perform a sensitivity analysis of the effect of pore structure on non-Darcy flow due to the extremely irregular structural nature. However, from the above results, a positive or negative correlation was found between the β factor, the SSA, and porosity. Here, we propose a new correlation, which contains the terms of SSA, porosity, and permeability, to describe the β factor. Furthermore, it meets the criterion of dimensional analysis, and is expressed as

$$\beta = af(\phi)(\frac{S}{K_d})^{\frac{1}{3}} \tag{15}$$

Where a equals 2.7×10^8; S denotes the SSA, um^{-1}; and $f(\phi)$ is a function of porosity, following the conclusions by scholars (Ergun, 1952; Yazdchi and Luding, 2012), which can be defined as a monotonically decreasing function, $f(\phi)=(1-\phi)/\phi^3$. Recently, Newman and Yin (Newman and Yin, 2013) provided a correlation, see Equation (16), from which it can be seen that the β factor has a positive relation with the $f(\phi)$ but has a negative relation with SSA. However, this is contrary to what was observed and to the conclusions of previous studies (Ergun, 1952; Yazdchi and Luding, 2012), and might need to be corrected.

$$\beta\sqrt{K_d} = 0.00993 f(\phi)\left(K_d S^2\right)^{-1/2} \tag{16}$$

In which, $f(\phi)=\phi/\sqrt{1-\phi}$ is a monotonically increasing function when ϕ is between 0 and 1.

Similar to the results from Figure 4 and 5, the models with more heterogeneous structure exhibit an earlier non-Darcy regime and lower permeability. Additionally, the results presented in Figure 6b show a good fit when using Equation (15) from geometry C1~C8, but a remarkable deviation from the fitting line was viewed for R1~R4. This implies that for the simple geometries, C1~C8 for example, the β factor being characterized using SSA, Darcy permeability, and SSA might be sufficient, while for the model with a complicated heterogeneity, described only by these parameters may be found wanting and might need to have more parameters incorporated.

It should be noted that there are still some limitations within in our work, and the developed correlation may not be directly used to predict non-Darcy flow characteristic. One of the reasons for that is the correlation is based on 2D

simulations, which is inconsistent with realistic porous media. Hence, the possibility of application in the 3D medium remains open. As such, the models used in this study for the investigation of the effects of pore structure on non-Darcy flow are far from sufficient if one intends to propose a general equation to β factor. Furthermore, characterization of pore structures only through the use of SSA, porosity, and permeability are also insufficient; some key factors, such as pore-throat size distribution, coordination number, the relative position of pore clusters, and two/three even higher-point correlation function might be needed to account for the complex structure (Rabbani et al., 2016; Sharqawy, 2016; Tahmasebi and Sahimi, 2013). However, the question remains that these parameters are hard to determine experimentally but procurement through the digital rock physics method is possible. In other words, an accurate correlation which involves multifold impacts to elucidate the inertial effect would not be able to be widely used in relevant industries. The main objective of this study is thus to highlight the effect of pore structure on inertial flow in porous media, and the development of a strong correlation is of huge practical value, and as such, will be conducted in our future investigations.

3.4 Analysis of inertial flow modes

As mentioned before, non-Darcy flows in porous media are highly dependent of the medium structure, where higher complexity magnifies fluid inertial effects (Nissan and Berkowitz, 2018). Furthermore, this effect triggers various flow patterns in pore space and the apparent permeability and tortuosity changes accordingly, as the Reynolds number increases.

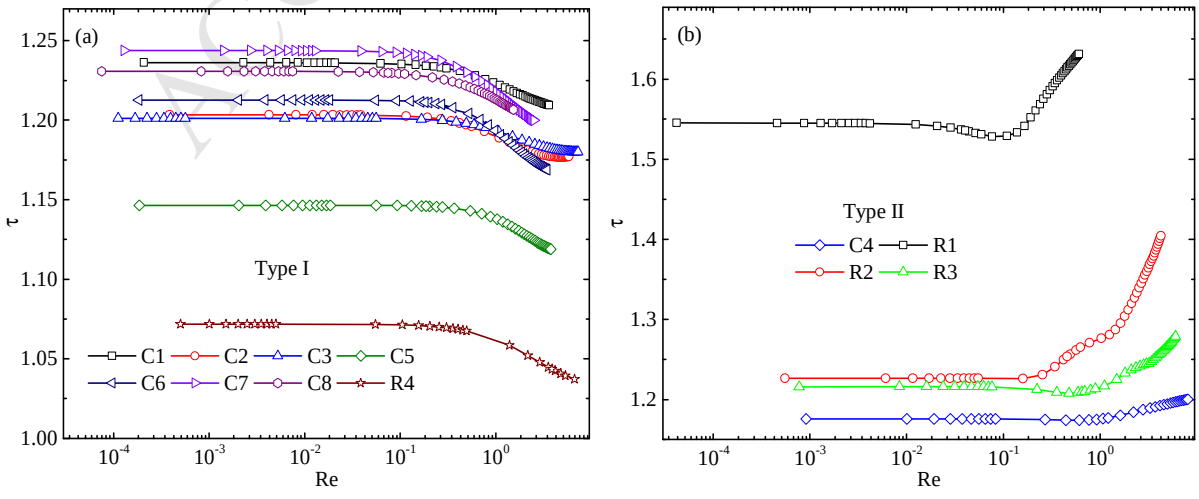

Fig.7. Two types of trends of variation in tortuosity with an increase in the Reynolds number. (a) a gradual decline in tortuosity; (b) a gradual increment in tortuosity.

The variation of apparent permeability has been discussed before, when the flow regime transitions from linear to nonlinear, and the feature of tortuosity was presented in this section. Figure 7 displays the variation trends of tortuosity versus the Reynolds number. Surprisingly, the variation trend of tortuosity for these models can be classified into two types; when the non-Darcy flows appear, the Type I curve shows a monotonically increasing tendency while Type II shows a decreasing one. Indeed, Type II has been demonstrated by some researchers (Chukwudozie and Tyagi, 2013; Chukwudozie et al., 2012; Kakouei et al., 2017; Muljadi et al., 2016), and the main cause for that will be elaborated in detail furthermore in the paper. However, as pointed out in the introduction, the Type I curve is only discovered in the work of Yazdchi and Luding (Yazdchi and Luding, 2012), but they did not provide a reasonable explanation for that. Here, this rather contradictory result will be clarified by a visualization analysis of flow modes in the model R4, C4 and R1. First, from the point view of mathematics, see Equation (14), the intrinsic velocity vector **u** would consist of the components along the X and Y direction. Hence, the decrease in tortuosity means the contribution of fluid velocity of X component becomes more significant. On the contrary, the increase in tortuosity indicates the larger portion of the Y component with respect to the velocity vector.

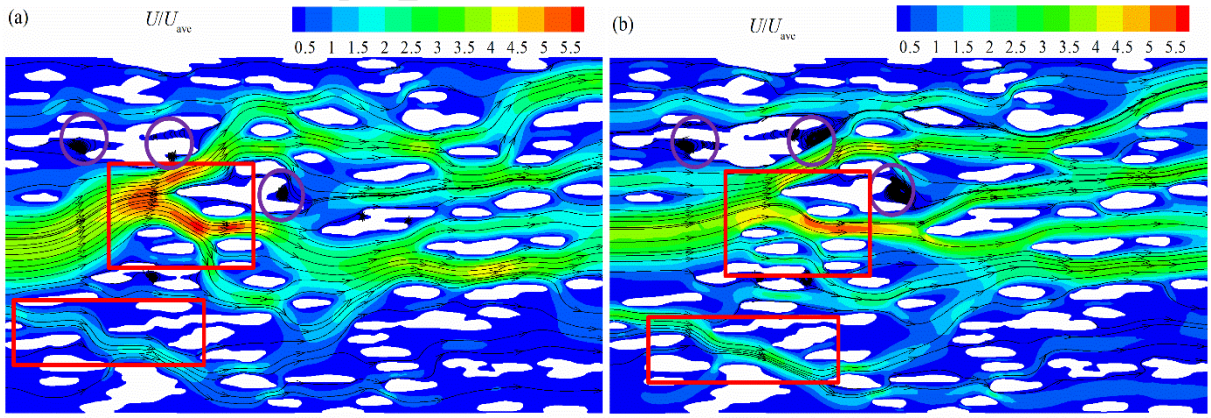

Fig.8. Plots of velocity distribution within R4 at specific points, with the legend being denoted by U/U_{ave}, where U_{ave} is the average velocity through the entire porous medium; (a) the Darcy regime (Re=5.7×10^{-3}) and (b) the non-Darcy regime (Re=6.68).

Figure 8 depicts the fluid velocity fields for R4 at two different Reynolds number, and it is observed that at the Darcy regime, the fluid spreads evenly through the pore space in the area where a local high-velocity zone exists, within the flow domain (marked by a large rectangle). However, with increasing the Reynolds number, the high-speed region within Figure 8a is shifted to a straight pore throat (see the red rectangle in Figure 8b), and an apparent concentration of fast flow appears and the sweeping efficiency of fluid is also reduced. This finding is qualitatively in line with the findings of previous studies (Muljadi et al., 2016; Newman and Yin, 2013). Additionally, another high-rate zone takes place in the lower left of the model. These phenomena can be explained by the “inertial cores” mechanism (Dybbs and Edwards, 1984). Furthermore, some small steady eddies emerge within pore spaces, even at Darcy flow conditions, due to the confined pores which is only swept by flow recirculation (marked by the purple circles), at higher Reynolds number more intensive eddies occurs. The generated vortex is detrimental to the fluid flow and makes the flow path more tortuous. Overall, the variation of tortuosity for a porous medium is derived as an outcome of multiple mechanisms acting together. The decreased tortuosity for Type I reveals that the total flow flux mainly comes from the contribution of these enhanced flow paths, and the effect of inertial core outweighs the effect of steady eddies.

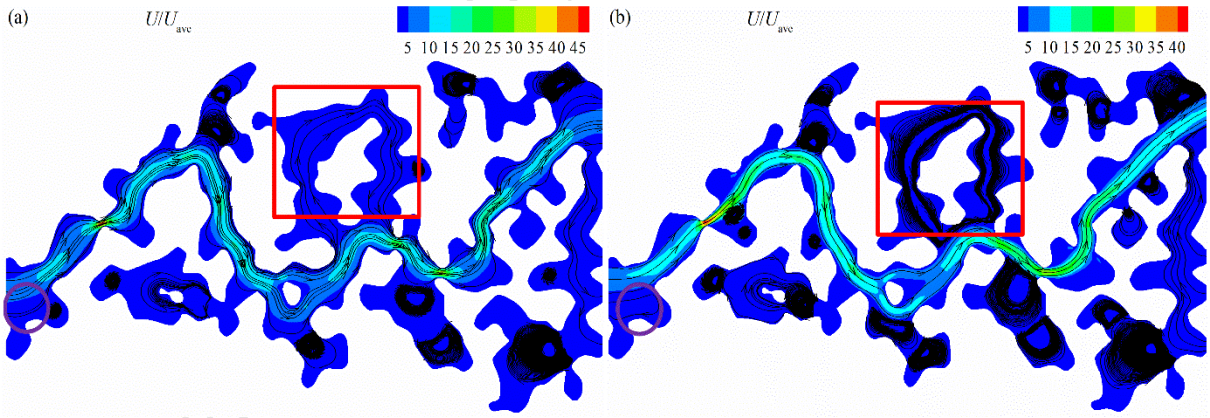

Fig.9. Plots of velocity distribution of within R1 at specific points; (a) the Darcy regime (Re=1.1×10^{-4}) and (b) the non-Darcy regime (Re=1.37).

The velocity fields for R1 at different regimes are presented in Figure 9. Similar to the case of R4, some eddies were also observed in the Darcy regime because of the intricate pore structure then grows as the Reynolds number increases (see the purple circle). These eddies usually emerge where obstacles touch and the flow cannot transverse effectively, as

pointed out by Fourar et al.(Fourar et al., 2004). In addition, another observation made, in relation to Figure 13, is that a reversal flow occurs (denoted by a red rectangle), i.e., at higher Reynolds number, the flow direction is shifted to the opposite direction and the values of the local velocities become negative, which leads to the increase in tortuosity. Furthermore, we also illustrated the velocity distribution of C4, and from Figure 10 we can conclude that the gradual deviation from Darcy's law is due to the dynamic growth of flow eddies and some new preferential flow paths. Despite the distribution of streamlines along the direction orthogonal toward the direction of applied pressure becoming more homogeneous, the existence of fluid vortex may result in the increase of tortuosity for C4.

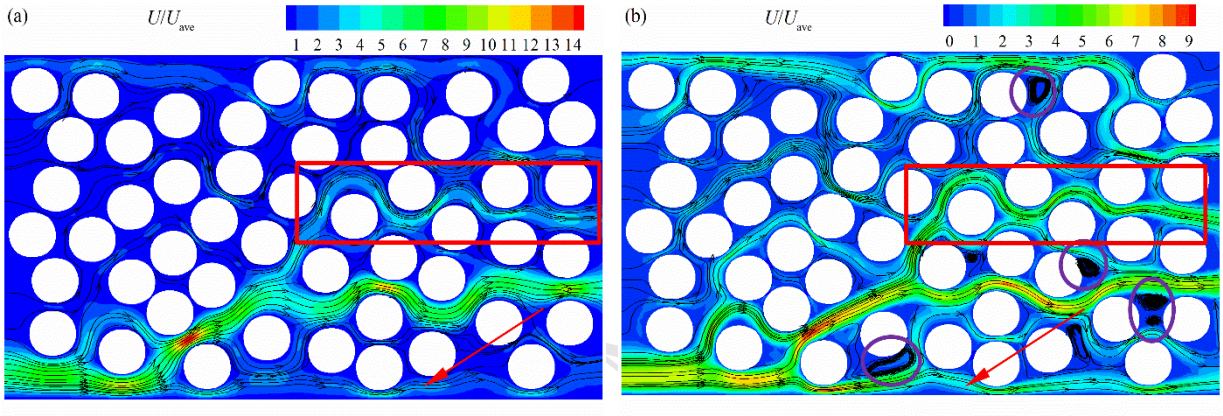

Fig.10. Plots of velocity distribution of within C4 at specific points; (a) the Darcy regime ($Re=9.4\times10^{-4}$) and (b) the non-Darcy regime (Re=6.1).

The LBM simulations at the pore scale indicate that the non-Darcy flow in porous media is collectively controlled by several mechanisms, as one alone cannot be responsible for the macroscopic behavior of fluid flow. We suggest that the inertial core effect in a large channel will lead to a more homogeneous flow and decrease the tortuosity, while for relatively intricate porous models, the steady eddy and reversal flow results from the drag force will make the flow paths more tortuous. Indeed, the features of inertial flow are closely related to the pore structure of the model; one must have a clear recognition of the porous model before carrying out the investigation of non-Darcy flow in porous media. In addition, we also speculate that these effects would also appear in 3D porous models, which might have a faster transformation from Darcy regimes to non-Darcy regimes, as 3D flow paths are more complicated. Besides, to form a percolated pore space, 3D geometry may need a lower porosity compared to the 2D models. Clearly, a study of

non-Darcy flows in various 3D models is worth being conducted in the future.

4. Conclusion

In this study, we performed a series of non-Darcy flow simulations in various porous models through the use of the lattice Boltzmann method, and the capability of two non-Darcy correlations in porous media, the effect of pore structure on non-Darcy flow, and the types of non-Darcy flow patterns were revealed based on the simulation results. The main conclusions of this study are as follows.

(1) The cubic law is only valid in representing the early stages of non-Darcy flows in porous media; beyond this regime, the inertia-dominated flow yields to the quadratic correction, which has a better accuracy than the cubic term. On the whole, the characterization of non-Darcy flows using the quadratic correction is acceptable, especially for the porous media with higher complexity.

(2) The features of non-Darcy flow are greatly affected by the pore structure of a porous medium. Generally, more heterogeneous pore models always have a faster cessation and a larger β factor. To be specific, when fixing other structural parameters, the porous media with lower porosity and higher specific surface area would have a more tortuous pore space, thus increasing the effect of fluid inertia.

(3) We also attempted to predict the β factor using some relevant structural properties; the results indicated that for simple porous media, several parameters may be adequate while more parameters would be needed to determine the β factor for the heterogeneous porous models.

(4) The non-Darcy flow that occurred in porous media was collectively controlled by several mechanisms. Through increasing the flow rate, the inertial core effect in a large channel will lead to a more homogeneous and less tortuous flow, while in porous models with a complicated pore space, the steady eddy and reversal flow resulting from the drag force will make the flow paths more tortuous. The gradual increase, or decrease, of tortuosity for a porous medium in non-Darcy flow regime thus reflects the combined actions of such mechanisms.

Acknowledgements

The authors would like to thank National Natural Science Foundation of China (Grant No. 51504265, 51474222 and 51774298) and PetroChina Innovation Foundation (2017D-5007-0205) for the financial support. We also appreciate Dr. Huawei Zhao from SINOPEC Petroleum Exploration and Production Research Institute for his kind help in coding the LB schemes.

Appendix A. Supplementary material

All the geometry models used in the present work and validation of our numerical models can be found in supporting information.

References

Andrade Jr, J., Costa, U., Almeida, M., Makse, H. and Stanley, H., 1999. Inertial effects on fluid flow through disordered porous media. Phys. Rev. Lett., 82(26): 5249.

Arabjamaloei, R. and Ruth, D., 2017. Numerical study of inertial effects on permeability of porous media utilizing the Lattice Boltzmann Method. J. Nat. Gas Sci. Eng., 44: 22-36.

Balhoff, M.T. and Wheeler, M.F., 2009. A predictive pore-scale model for non-Darcy flow in porous media. SPE J., 14(04): 579-587.

Bhatnagar, P.L., Gross, E.P. and Krook, M., 1954. A Model for Collision Processes in Gases. I. Small Amplitude Processes in Charged and Neutral One-Component Systems. Phys. Rev., 94(3): 511-525.

Chen, L., Kang, Q., Mu, Y., He, Y.-L. and Tao, W.-Q., 2014. A critical review of the pseudopotential multiphase lattice Boltzmann model: Methods and applications. Int. J. Heat Mass Transfer, 76: 210-236.

Chen, L. et al., 2015. Nanoscale simulation of shale transport properties using the lattice Boltzmann method: permeability and diffusivity. Scientific Reports, 5: 8089.

Chukwudozie, C. and Tyagi, M., 2013. Pore scale inertial flow simulations in 3 - D smooth and rough sphere packs using lattice Boltzmann method. AlChE J., 59(12): 4858-4870.

Chukwudozie, C., Tyagi, M., Sears, S. and White, C., 2012. Prediction of non-Darcy coefficients for inertial flows through the castlegate sandstone using image-based modeling. Transport Porous Med., 95(3): 563-580.

Comiti, J., 2000. Experimental characterization of flow regimes in various porous media-III: limit of Darcy's or creeping flow regime for Newtonian and purely viscous non-Newtonian fluids. Chemical Engrg. Sci., 55: 3057-3061.

Cooper, J., Wang, X. and Mohanty, K., 1999. Non-Darcy-flow studies in anisotropic porous media. SPE J., 4(04):

334-341.

Duda, A., Koza, Z. and Matyka, M., 2011. Hydraulic tortuosity in arbitrary porous media flow. Phys. Rev. E, 84(3): 036319.

Dybbs, A. and Edwards, R., 1984. A new look at porous media fluid mechanics—Darcy to turbulent, Fundamentals of transport phenomena in porous media. Springer, pp. 199-256.

Ergun, S., 1952. Fluid flow through packed columns. Chem. Eng. Prog., 48: 89-94.

Feng, Y., Han, K. and Owen, D., 2007. Coupled lattice Boltzmann method and discrete element modelling of particle transport in turbulent fluid flows: Computational issues. International Journal for Numerical Methods in Engineering, 72(9): 1111-1134.

Firdaouss, M., Guermond, J.-L. and Le Quéré, P., 1997. Nonlinear corrections to Darcy's law at low Reynolds numbers. J. Fluid Mech., 343: 331-350.

Forchheimer, P., 1901. Wasserbewegungdurchboden, 45.

Fourar, M., Radilla, G., Lenormand, R. and Moyne, C., 2004. On the non-linear behavior of a laminar single-phase flow through two and three-dimensional porous media. Adv. Water. Resour., 27(6): 669-677.

Friedel, T. and Voigt, H.-D., 2006. Investigation of non-Darcy flow in tight-gas reservoirs with fractured wells. J. Petrol Sci. Eng., 54(3): 112-128.

Guo, Z.-L., Zheng, C.-G. and Shi, B.-C., 2002a. Non-equilibrium extrapolation method for velocity and pressure boundary conditions in the lattice Boltzmann method. Chinese Phys., 11(4): 366.

Guo, Z., Zheng, C. and Shi, B., 2002b. Discrete lattice effects on the forcing term in the lattice Boltzmann method. Phys. Rev. E, 65(4): 046308.

Hill, R.J., Koch, D.L. and Ladd, A.J.C., 2001. The first effects of fluid inertia on flows in ordered and random arrays of spheres. J. Fluid Mech., 448: 213-241.

Huang, H., Huang, J.-J. and Lu, X.-Y., 2014. Study of immiscible displacements in porous media using a color-gradient-based multiphase lattice Boltzmann method. Comput. Fluids, 93: 164-172.

Kakouei, A., Vatani, A., Rasaei, M., Sola, B.S. and Moqtaderi, H., 2017. Cessation of Darcy regime in gas flow through porous media using LBM: Comparison of pressure gradient approaches. J. Nat. Gas Sci. Eng., 45: 693-705.

Koch, D.L. and Ladd, A.J., 1997. Moderate Reynolds number flows through periodic and random arrays of aligned cylinders. J. Fluid Mech., 349: 31-66.

Koponen, A., Kataja, M. and Timonen, J., 1996. Tortuous flow in porous media. Phys. Rev. E, 54(1): 406.

Ma, H. and Ruth, D., 1993. The microscopic analysis of high Forchheimer number flow in porous media. Transport Porous Med., 13(2): 139-160.

Macini, P., Mesini, E. and Viola, R., 2011. Laboratory measurements of non-Darcy flow coefficients in natural and artificial unconsolidated porous media. J. Petrol Sci. Eng., 77(3-4): 365-374.

Marusic-Paloka, E. and Mikelic, A., 2000. The derivation of a nonlinear filtration law including the inertia effects via homogenization. Nonlinear Analysis-Series A Theory and Methods and Series B Real World Applications, 42(1): 97.

Mei, C. and Auriault, J.-L., 1991. The effect of weak inertia on flow through a porous medium. J. Fluid Mech., 222: 647-663.

Miskimins, J.L., Lopez, H.D.J. and Barree, R.D., 2005. Non-Darcy flow in hydraulic fractures: does it really matter?, SPE Annual Technical Conference and Exhibition. Society of Petroleum Engineers.

Muljadi, B.P., Blunt, M.J., Raeini, A.Q. and Bijeljic, B., 2016. The impact of porous media heterogeneity on non-Darcy flow behaviour from pore-scale simulation. Adv. Water. Resour., 95: 329-340.

Narváez, A., Yazdchi, K., Luding, S. and Harting, J., 2013. From creeping to inertial flow in porous media: a lattice Boltzmann–finite element study. Journal of statistical mechanics: theory and experiment, 2013(02): P02038.

Newman, M.S. and Yin, X., 2013. Lattice Boltzmann simulation of non-Darcy flow in stochastically generated 2D porous media geometries. SPE J., 18(1): 12-26.

Nissan, A. and Berkowitz, B., 2018. Inertial Effects on Flow and Transport in Heterogeneous Porous Media. Phys. Rev. Lett., 120(5): 054504.

Qian, Y.H., Humières, D.D. and Lallemand, P., 1992. Lattice BGK Models for Navier-Stokes Equation. EPL (Europhysics Letters), 17(6): 479.

Rabbani, A., Ayatollahi, S., Kharrat, R. and Dashti, N., 2016. Estimation of 3-D pore network coordination number of rocks from watershed segmentation of a single 2-D image. Adv. Water. Resour., 94: 264-277.

Ramirez, B.A., Kazemi, H., Ozkan, E. and Al-Matrook, M.F., 2007. Non-Darcy flow effects in dual-porosity, dual-permeability naturally fractured gas condensate reservoirs, SPE Annual Technical Conference and Exhibition. Society of Petroleum Engineers.

Sharqawy, M.H., 2016. Construction of pore network models for Berea and Fontainebleau sandstones using non-linear programing and optimization techniques. Adv. Water. Resour., 98: 198-210.

Tahmasebi, P. and Sahimi, M., 2013. Cross-correlation function for accurate reconstruction of heterogeneous media. Phys. Rev. Lett., 110(7): 078002.

Thauvin, F. and Mohanty, K., 1998. Network modeling of non-Darcy flow through porous media. Transport Porous Med., 31(1): 19-37.

Wang, M., Wang, J., Pan, N. and Chen, S., 2007. Mesoscopic predictions of the effective thermal conductivity for microscale random porous media. Phys. Rev. E, 75(3): 036702.

Wang, X., Thauvin, F. and Mohanty, K., 1999. Non-Darcy flow through anisotropic porous media. Chem. Eng. Sci., 54(12): 1859-1869.

Yazdchi, K. and Luding, S., 2012. Towards unified drag laws for inertial flow through fibrous materials. Chem. Eng. J., 207: 35-48.

Yazdchi, K., Srivastava, S. and Luding, S., 2010. On the transition from creeping to inertial flow in arrays of cylinders, ASME 2010 International Mechanical Engineering Congress and Exposition. American Society of Mechanical Engineers, pp. 767-772.

Yazdchi, K., Srivastava, S. and Luding, S., 2011. Microstructural effects on the permeability of periodic fibrous porous media. Int. J. Multiphase Flow, 37(8): 956-966.

Yazdchi, K., Srivastava, S. and Luding, S., 2012. Micro–macro relations for flow through random arrays of cylinders. Composites Part A: Applied Science and Manufacturing, 43(11): 2007-2020.

Yu, Z. and Fan, L.-S., 2010. Multirelaxation-time interaction-potential-based lattice Boltzmann model for two-phase flow. Phys. Rev. E, 82(4): 046708.

Zeng, Z. and Grigg, R., 2006. A Criterion for Non-Darcy Flow in Porous Media. Transport Porous Med., 63(1): 57-69.

Zhao, H., Ning, Z., Kang, Q., Chen, L. and Zhao, T., 2017. Relative permeability of two immiscible fluids flowing through porous media determined by lattice Boltzmann method. Int. Commun. Heat Mass, 85: 53-61.

Zhao, J. et al., 2018a. The Effect of Wettability Heterogeneity on Relative Permeability of Two‐Phase Flow in Porous Media: A Lattice Boltzmann Study. Water Resour. Res., 54(2): 1295-1311.

Zhao, J. et al., 2018b. Lattice Boltzmann simulation of liquid flow in nanoporous media. Int. J. Heat Mass Transfer, 125: 1131-1143.

Zhao, T., Zhao, H., Ning, Z., Li, X. and Wang, Q., 2018c. Permeability prediction of numerical reconstructed multiscale tight porous media using the representative elementary volume scale lattice Boltzmann method. Int. J. Heat Mass Transfer, 118: 368-377.

Highlights:

Non-Darcy flows in porous media are simulated using the lattice Boltzmann method.

The effects of pore structure on non-Darcy flow are studied.

The flow patterns of the fluid in the non-Darcy regime are elaborated.